The interface structural, electronic and optical properties of ZnO nanowires/Graphene nanohybrid (ZnO NWs/G)

Experimental and theoretical DFT investigations

Boukhoubza, Issam; Achehboune, Mohamed; Derkaoui, Issam; Apostol, Mariana Mihaela; Basyooni, Mohamed A.; Khenfouch, Mohammed; Nedelcu, Liviu; Enculescu, Ionut; Matei, Elena

DOI
10.1016/j.jallcom.2023.173109

Publication date
2024

Document Version
Final published version

Published in
Journal of Alloys and Compounds

Journal of Alloys and Compounds 976 (2024) 173109

Contents lists available at ScienceDirect

Journal of Alloys and Compounds

journal homepage: www.elsevier.com/locate/jalcom

The interface structural, electronic and optical properties of ZnO nanowires/Graphene nanohybrid (ZnO NWs/G): Experimental and theoretical DFT investigations

Issam Boukhoubza [a], Mohamed Achehboune [b], Issam Derkaoui [c], Mariana Mihaela Apostol [a,d], Mohamed A. Basyooni [e,f], Mohammed Khenfouch [g], Liviu Nedelcu [a], Ionut Enculescu [a], Elena Matei [a,*]

[a] National Institute of Materials Physics, Atomistilor 405A, 077125 Magurele, Romania
[b] Laboratoire de Physique du solide, Namur Institute of Structured Matter, University of Namur, Rue de Bruxelles 61, 5000 Namur, Belgium
[c] Laboratory of Solid state Physics, Faculty of Sciences Dhar el Mahraz, University Sidi Mohammed Ben Abdellah, PO Box 1796 Atlas, Fez 30000, Morocco
[d] University Politehnica of Bucharest, Faculty of Chemical Engineering and Biotechnologies, Gheorghe Polizu 1-7, 011061 Bucharest, Romania
[e] Department of Nanotechnology and Advanced Materials, Graduate School of Applied and Natural Science, Selçuk University, Konya 42030, Turkey
[f] Department of Precision and Microsystems Engineering, Delft University of Technology, Mekelweg 2, 2628 CD Delft, the Netherlands
[g] Laboratory of Materials, Electrical Systems, Energy and Environment (LMS3E), Materials and Energy Engineering team, Faculty of Applied Sciences, Department of Physics, Ait Melloul, Ibn Zohr University, 86153 Agadir, Morocco

ARTICLE INFO

Keywords:
ZnO NWs/Graphene
Electrochemical deposition
GGA-PBE+U
Optoelectronic properties

ABSTRACT

In this work, a ZnO nanowires/graphene nanohybrid was synthesized by a three steps approach. Copper substrates were covered with graphene by chemical vapor deposition, further ZnO nanowires were electrochemically deposited on the as grown graphene on copper and finally a transfer process was employed for moving the heterostructure onto a different substrate. A comprehensive structural analysis which included scanning electron microscopy, X-ray diffraction and Raman measurements revealed that the ZnO nanowires crystallize in wurtzite structure perpendicular to graphene, the process leading to the formation of a nanohybrid heterostructure. The band gap energy of the ZnO nanowires deposited on graphene was estimated to be 3.11 eV, as calculated from the reflectance spectrum analysis. The GGA-PBE+U within Grimme (DFT-D) approach was used to provide an accurate description of the interface structure in terms of electronic and optical properties, confirming that the decrease in the band gap energy of ZnO nanowires is caused by the interaction with the graphene surface. The findings of this study could serve as an experimental and theoretical reference for upcoming studies on ZnO NWs/Graphene nanohybrid-based optoelectronic applications.

1. Introduction

Low dimensional carbon materials have opened new potential lucrative pathways in scientific and technological advancement due to their unique properties. In particular, graphene (G) is a 2D material that has generated a great deal of interest due to a set of specific characteristics, consequence of its low dimensionality. These characteristics include high mechanical strength and flexibility, high charge carrier mobility, excellent transparency and thermal conductivity [1–3]. Due to these outstanding properties, graphene is considered as a promising functional material in many applications, including photocatalysis, sensors and biosensors, energy storage, electronic and optoelectronic devices [4–9]. One of the preferred methods of producing good quality (high conductivity and high transparency) graphene sheets is the chemical vapor deposition (CVD) on copper substrates [10]. The CVD route enables the production of high-quality graphene, i.e. low concentration of defects and well controlled structure and morphology [11].

ZnO is a wide bandgap (3.37 eV) semiconductor with high electron mobility, high transparency, wide UV absorption range and high exciton binding energy [12,13]. ZnO occurs abundantly in nature and is non-toxic. Zinc oxide is a polymorphic material at nanoscale, various methods of synthesis leading to the fabrication of different

* Corresponding author.
E-mail address: elena.matei@infim.ro (E. Matei).

https://doi.org/10.1016/j.jallcom.2023.173109
Received 7 July 2023; Received in revised form 17 November 2023; Accepted 8 December 2023
Available online 12 December 2023

nanostructures, such as nanowires [14], nanorods [15], nanotubes [16], nanoflowers [17] nanosheets [18]. These semiconducting nanostructures can be further employed as building blocks in fabricating a variety of electronic or optoelectronic devices with morphology/dimensionality tailored properties.

A ZnO/Graphene heterostructure is an interesting combination of materials due to the fact that both its components present excellent electronic and optoelectronic properties and thus open the path towards a variety of applications, such as photocatalysis, supercapacitors, sensors, and solar cells [19–22]. Moreover, the strong electronic combination between the nanostructured ZnO and the low dimensionality carbon material in a nanohybrid system can dramatically change the ZnO band structure. By tuning the process parameters for the ZnO growing on top of a graphene covered substrate, the morphology/aspect ratio, the orientation, and the density of the resulting ZnO nanostructures can be controlled [23].

However, our comprehension of the atomic-level details at the interface between graphene and ZnO remains incomplete. Although a prior theoretical investigation demonstrated enhanced field emission properties in ZnO/graphene composites [24,25], there remains a lack of a comprehensive understanding of how the interface impacts the electronic characteristics of graphene when subjected to ZnO modification. In semiconductor research, a material's structure plays a pivotal role in dictating its electronic behavior, and in the context of heterostructures, the interfaces between semiconductors wield significant influence over their properties. Factors such as stacking order, dislocation, interfacial atom species, and boundary arrangements all exert substantial effects on the electronic and optoelectronic properties. The wave functions of these interfacial atoms determine the occurrence of chemical bonds or physical adsorption, while the relative positions of electronic bands on both sides of the interface profoundly influence conductivity and charge transfer. Understanding this intricate relationship between interface structure and electronic properties is imperative for the advancement of electronic applications. Consequently, to harness the potential of this hybrid structure composed of two distinct nanostructures, it is essential to establish a theoretical model that delineates its specific properties and compares them with experimental results. In pursuit of this objective, Density Functional Theory calculations with Hubbard U correction (DFT+U) stand out as a potent methodology that offers profound insights into the electronic structure and optical properties of the synthesized nanohybrid material at the atomic level [26–29].

The present work reports the growth of ZnO nanowires (NWs) on CVD-graphene/Cu using an electrochemical deposition method, followed by the transfer of this hybrid material from copper to a SiO_2/Si substrate via electrochemical delamination. A comprehensive analysis, employing scanning electron microscopy (SEM), X-ray diffraction (XRD), Raman spectroscopy, as well as reflectance spectroscopy (R%), was used to explore the influence of the graphene substrate on the structural, micromorphological, and optical properties of the ZnO nanowires embedded in this particular heterostructure. Further, we provide a theoretical investigation employing density functional theory with Hubbard U correction (DFT+U) to elucidate the impact of the graphene substrate on the structural, electronic, and optical characteristics of ZnO nanowires. This research contributes to advancing our understanding of the promising electronic applications and fundamental properties of ZnO NWs/graphene nanohybrid, addressing the pressing need for both theoretical modeling and experimental validation in this emerging field.

2. Experimental and theoretical details

2.1. Synthesis of ZnO nanowires/CVD-graphene

Graphene was synthesized on copper foil substrates through the chemical vapor deposition (CVD) method using a AS-One Rapid Thermal Processor system. Initially, the Cu substrates, sized at 2 × 2 cm^2 with a thickness of 25 μm, were subjected to ultrasonic cleaning in acetone and isopropyl alcohol for a duration of 10 min to eliminate any organic residues. The first phase of the process involves annealing of the Cu substrate in a hydrogen atmosphere for 30 min at a pressure of 10 millibars to reduce existing oxides and promote the growth of larger copper crystallites [30]. The subsequent step consists in the actual growth of graphene in a mixed gas atmosphere of hydrogen (H_2) and methane (CH_4) with a flow ratio of 10:25, respectively, for a duration of 10 min. The final stage of the process includes rapid cooling of the sample using an argon (Ar) atmosphere. Subsequently, the growth of ZnO nanowires on CVD-Graphene/Cu substrates was performed using the electrochemical deposition method as we have done in our previous work [23]. Further, a film of polymethyl methacrylate (PMMA) was deposited by spin coating in order to protect the ZnO NWs/CVD-graphene during manipulation and thus to facilitate the transfer. A 4,5% PMMA solution was dropped on the ZnO NWs/CVD-graphene/Cu, the process being carried out at 3000 rpm for 40 s. During a subsequent heating step, at 120 °C for 2 min the PMMA film solidified. Finally, the transfer of ZnO NWs/G nanohybrid deposited on a SiO_2/Si surface was carried out according to a method well described in the literature for graphene method based on the electrochemical delamination from the metallic substrate [31]. In order, to initiate the delamination, a potential of − 1.8 V vs. a Red Rod reference electrode was applied while the film was slowly dipped into the electrolyte (0.5 M NaCl aqueous solution), resulting in the complete separation of the PMMA/ ZnO NWs/G film from the Cu substrate. The typical time required for separation was about 2 min. The process leads to the PMMA coated ZnO NWs/G floating on the surface of the electrolyte solution. Afterwards, the floating film was placed on a SiO_2/Si substrate, the PMMA being removed by dissolving it in acetone followed by thoroughly rinsing with isopropanol. The process of obtaining ZnO NWs/G nanohybrid on SiO_2/Si is schematically illustrated in Fig. 1.

2.2. Characterization

A Bruker D8 Advance diffractometer (Bruker AXS, Karlsruhe, Germany) using CuKα radiation (λ = 1.54178 Å) was employed to characterize the crystal structure of the films in the 20–70° range. For the morphology analysis of ZnO NWs/G/Cu and ZnO NWs/G/SiO_2/Si a Gemini 500 scanning electron microscope (Zeiss, Obercohen, Germany) was used. The Raman spectra of the ZnO nanowires/graphene were recorded using a LabRAM HR Evolution Raman spectrometer (Horiba Jobin-Yvon: Edison, Palaiseau, France), with a He–Ne laser emitting at 633 nm, focused by an Olympus 100 × objective on the surface of the film. A PerkinElmer Lambda 45 UV-Vis spectrophotometer (Waltham, Massachusetts, USA) was used to record the reflectance spectra.

2.3. Computational method

In the present study, the structure simulations and all the other properties were calculated using The Cambridge Serial Total Energy Package module (CASTEP) [32]. The correlation and exchange effects between electrons were considered with the generalized gradient approximation of Perdew-Burke-Ernzerhof [33] (GGA-PBE). Furthermore, the calculations were carried out using the ultra-soft plane wave pseudopotential method [34] with valence electron configurations of 4 $s^2 3d^{10}$ for Zn, 2 $s^2 2p^4$ for O, and 2 $s^2 2p^2$ for C to describe the interactions between the ionic core and the valence electrons and to allow the present calculation to be performed with a cut-off energy of 450 eV.

Furthermore, in the case of metal oxides, the on-site Coulomb interactions are notably strong for localized d and f electrons, but they are also significant for localized p orbitals. Using GGA or LDA methods often underestimates the band gap energy in these systems. Therefore, GGA+U had potentially improved the insufficient description of strongly localized electrons. In our study, the Hubbard U correction (GGA+*U*) was employed to enhance the accuracy of our electronic

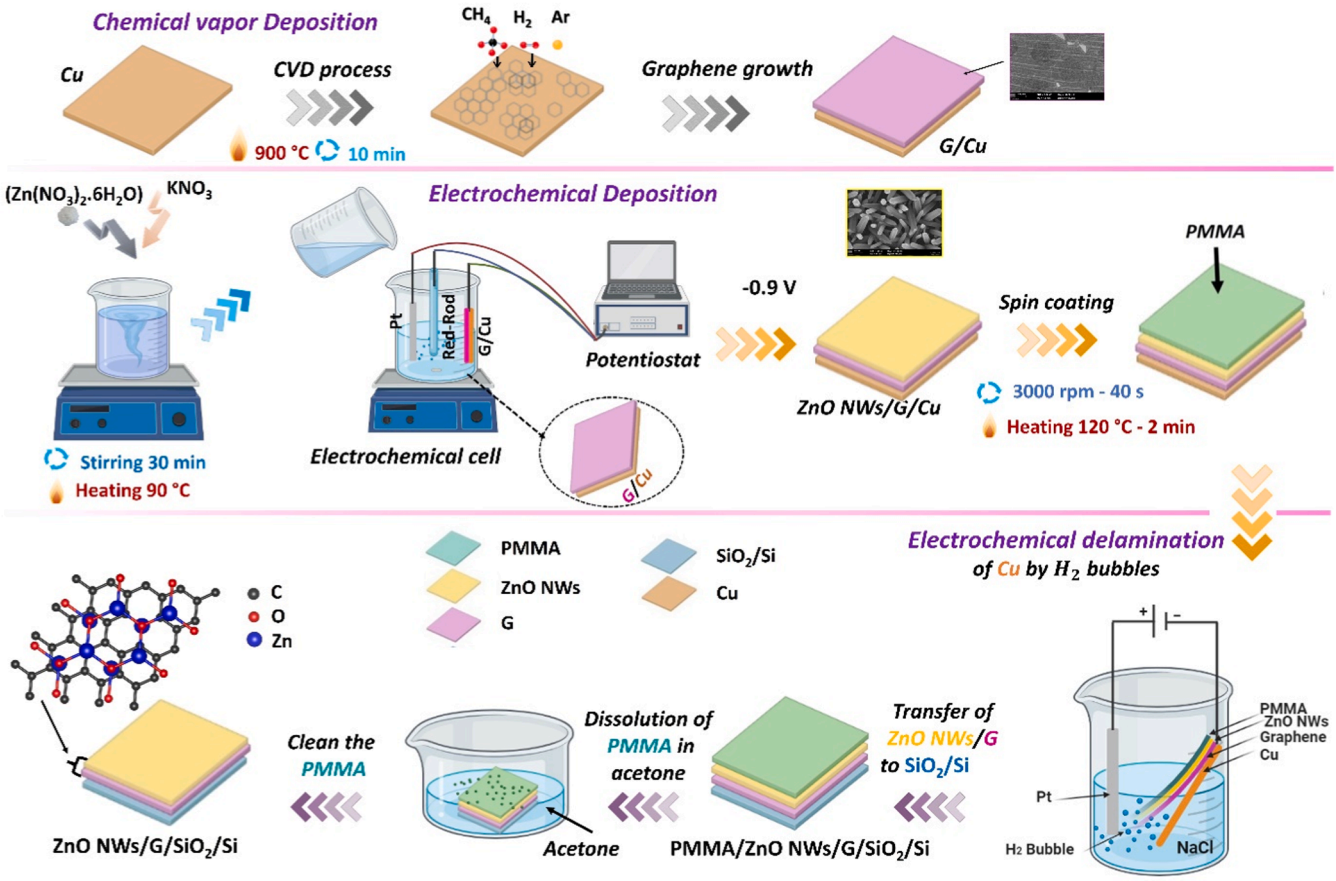

Fig. 1. Representation of CVD graphene growth, electrochemical deposition of ZnO NWs on G/Cu surface, and the ZnO NWs/G nanohybrid transfer process onto SiO_2/Si substrate by electrochemical delamination of the Cu substrate.

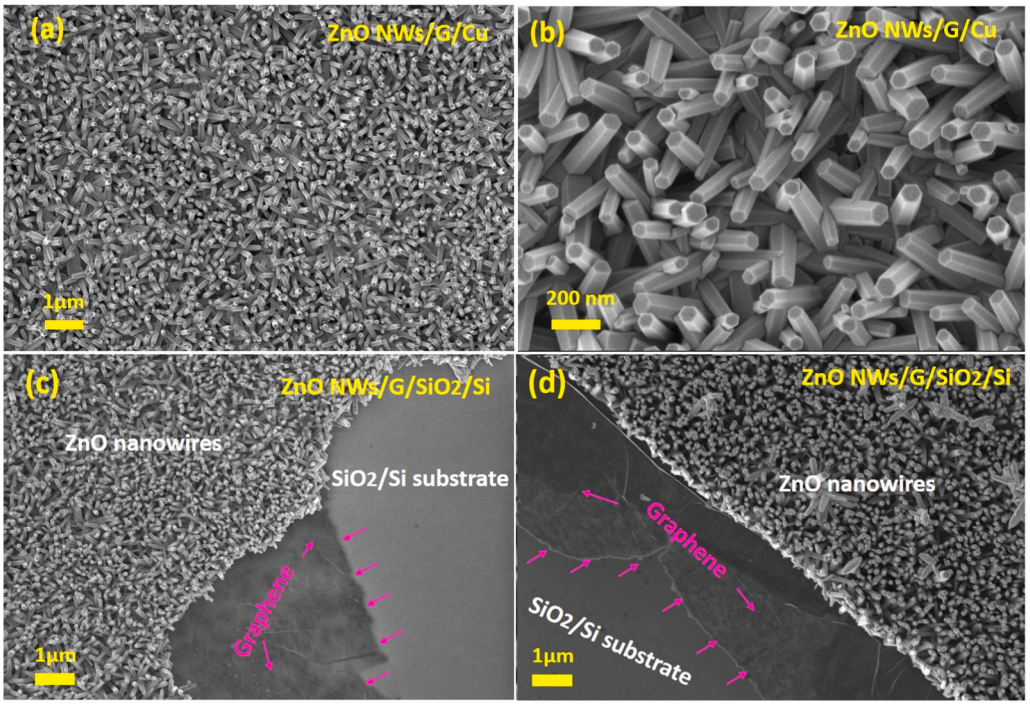

Fig. 2. SEM images of ZnO NWs deposited on G/Cu (a,b) and ZnO NWs/G transferred onto SiO_2/Si substrate (c,d).

structure calculations. We adopted specific values for U, set at 10 eV for Zn(3d) and 9 eV for O(2p), as reported in [35]. The Brillouin zone integrations generated automatically by the Monkhorst-Pack method were performed over a 5 × 5 × 4 grid size for pure ZnO and 6 × 6 × 1 grid size for a ZnO molecule adsorbed on the graphene layer. Furthermore, the Grimme's DFT+D2 method was employed to characterize the adsorption energies and to correct the intermolecular forces between ZnO and graphene. All the calculations were carried out with spin polarization; the convergence threshold for self-consistent iteration being fixed at 10^{-5} eV/atom, and the lattice constants and all atomic positions for each supercell being totally relaxed until the maximal force on each atom was less than 0.03 eV/Å, the internal stress was below 0.05 GPa, and the displacement of each atom was below 0.01 Å. Furthermore, a 3 × 3 graphene 2D structure was constructed with a k-point mesh of 6 × 6 × 1. A vacuum space of around 15 Å was employed to prevent inter-slab interactions.

3. Experimental results

3.1. Morphological characterization by SEM

Fig. 2(a, b) displays scanning electron microscopy (SEM) images, obtained at different magnifications for ZnO nanowires grown on graphene/Cu substrates. It can be seen that the ZnO nanowires are uniform and dense, completely covering the substrate. The average diameter and length of the nanowires are in the range of 20–40 nm and 100–300 nm, respectively. Most of the nanowires exhibit a hexagonal cross-section, both perpendicular and oblique angle orientations relative to the graphene/Cu substrate being observed (Fig. 2(b)). The differences in orientation are probably a consequence to the graphene's wavy structure, created during the CVD-growth [36]. Although controlled deposition of tailored, functional materials on graphene from an aqueous medium is a challenge, owing to the 2-dimensional material's highly hydrophobic surface, the electrochemical deposition method has successfully enabled the growth of ZnO nanowires [37]. Fig. 2(c-d) shows the images of ZnO NWs/graphene film transferred onto SiO_2/Si after delamination from the Cu substrate and PMMA removal. It can be observed that, the ZnO nanowires uniformly cover the graphene surface (see dark part in Fig. 2(c)) and that the high-quality graphene was still present after the transfer. Additionally, it should be noted that a relatively large-scale (few square centimeters), uniform, layer of graphene was coated by nanowires and manipulated in a controlled way. As can be easily seen in Fig. 2(c-d), the transfer of the ZnO NWs/G layer was successfully achieved without destroying the specific architecture of the heterostructure.

3.2. X-ray diffraction and Raman analysis

The X-ray diffraction patterns of ZnO NWs/G/Cu and ZnO NWs/G/SiO_2/Si heterostructures are shown in Fig. 3(a). For the ZnO NWs/ G/Cu sample, the characteristic peaks at 31.89° (100), 34.56° (002), 36.4° (101), 47.57° (102), 56.6° (110), 62.9° (103), and 68.07° (112) were observed, and correspond to crystal planes of a hexagonal wurtzite structure of ZnO (ICDD PDF no.00–036–1451) [35]. It is clear to see that the additional characteristic peaks appeared at 2θ = 43° and 51° are accounted for the reflections from the (111) and (200) planes of the copper substrate (ICDD PDF no. 04–009–2090) [38–40]. After the transfer of ZnO NWs/G on SiO_2/Si substrate, these two peaks disappeared completely only the similar peaks of ZnO being preserved comparing with the XRD data of ZnO NWs/G/Cu. Furthermore, it can be observed that the intensity of the (002) peak in both cases is the highest, which indicates that the ZnO nanowires have a preferential orientation on the c-axis direction. Generally, graphene has diffraction peaks at 26.2° and 44.3° [41]. These peaks were not detected in the present graphene containing heterostructure. This absence can be attributed to the strong crystallinity of ZnO nanowires within the nanohybrid, which weakens the diffraction patterns of carbon atoms in graphene [42]. Moreover, the ZnO NWs effectively covered the entire graphene surface, resulting in prominent diffraction peaks. This observation aligns with previous research, such as Yoo et al. findings, which noted that XRD peaks for graphene were challenging to detect due to the limited quantity and low diffraction intensity of graphene [43]. Additionally, Zeng et al. reported that the graphene derivatives-related peak becomes significantly weakened after the growth of nanowires, suggesting

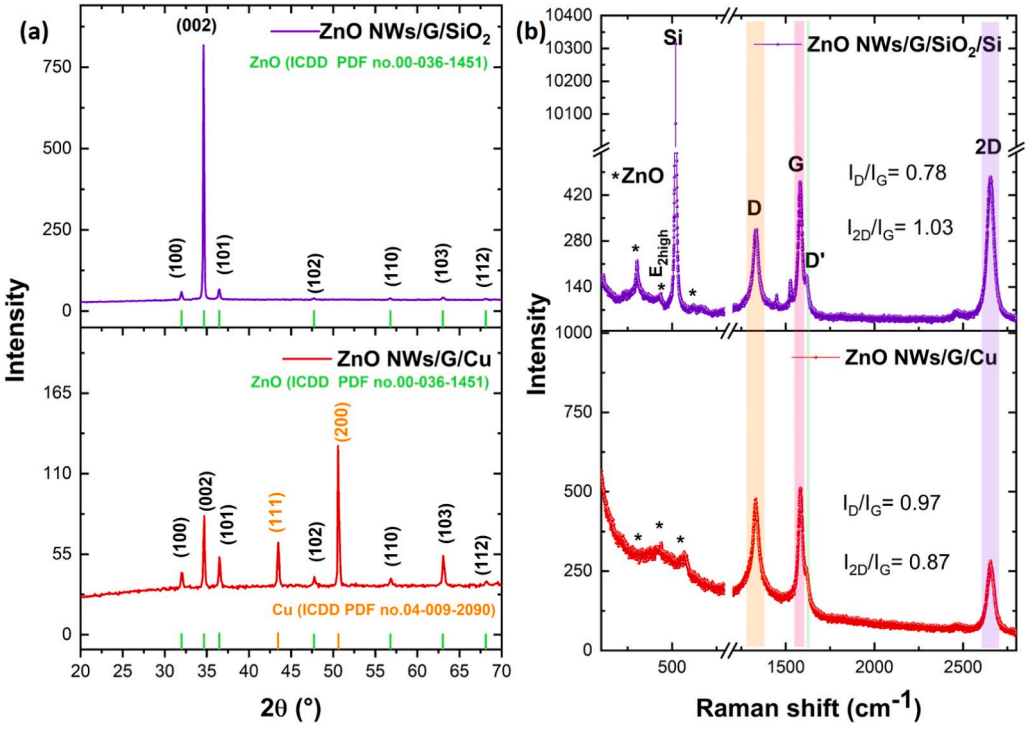

Fig. 3. (a) XRD Spectra and (b) Raman spectra of ZnO NWs/G/Cu and ZnO NWs/G/SiO_2/Si nanohybrid.

comprehensive coverage by ZnO nanowires [44].

Raman spectroscopy analysis of the ZnO NWs/G/Cu and ZnO NWs/G/SiO_2/Si using an excitation wavelength of 633 nm, showed the D, G, D′ and 2D graphene bands located at 1326, 1582, 1615 and 2658 cm^{-1}, respectively (Fig. 3(b)). According to the literature [45,46], the D band is related to a ring specific mode of vibration of sp^2 carbon, being also adjacent to a defect while the G band corresponds to the stretching of the C-C bond being observed in all sp^2-containing carbon materials. The weak 2D band is the second order of the D band but is related to the number of layers and not to a neighboring defect.

The characteristic Raman peaks for ZnO are: 291 cm^{-1} (multiple-phonon scattering processes), 429 cm^{-1} (E_{2high}) confirming the hexagonal wurtzite of ZnO nanowires, and 610 cm^{-1} (TA+A_1(LO)) [47,48]. The peak at 520 cm^{-1} corresponds to the phonon band of Si substrate [49]. These results confirm the uniform dispersion of ZnO nanowires on graphene layer.

The low D peak to G peak intensity ratio confirmed the presence of a graphene layer with low concentration of defects (for ZnO NWs/G/Cu (I_D/I_G = 0.97) and for ZnO NWs/G/SiO_2/Si (I_D/I_G = 0.78)), as seen in Fig. 3. Based on the I_{2D}/I_G intensity ratio, most of the graphene can be identified as being a bilayer graphene.

3.3. Diffuse reflectance analysis

The optical band gap value (E_g) of ZnO NWs/G nanohybrid was calculated from the slopes of the diffuse reflectance (R) spectra (Fig. 4 (a)) using the Kubelka-Munk function F(R) [50]:

$$F(R) = \frac{(1-R\%)^2}{2R\%}$$

By putting F(R) instead of α in the following equation:

$$(\alpha \times h\upsilon)^2 = A\left(h\upsilon - E_g\right)$$

where h is the Planck constant, ν is the photon's frequency, E_g is the band gap energy, and A is a constant. The measured reflectance spectra can be transformed to the corresponding absorption spectra by applying the Kubelka–Munk function. This yields the form :

$$(F(R) \times h\upsilon)^2 = A\left(h\upsilon - E_g\right)$$

Fig. 4(b) presents the E_g value of ZnO NWs/G nanohybrid calculated based on the linear part extrapolation of the function (F (R) × hυ)^2 which is the Tauc's plot equivalent, as a function of photon energy axis, hυ (eV). In this case, it was found that the ZnO nanowires layer has a band gap energy of 3.11 eV, which is lower than the bulk ZnO band gap (~ 3.37 eV). In the subsequent section, a theoretical study is presented, study which could be useful in order to understand at the atomic scale of the experimental observations.

4. Theoretical results

4.1. Adsorption of ZnO molecule on graphene layer

To understand the interaction mechanisms between ZnO and the graphene surface, we focus on the adsorption of ZnO on graphene. This interaction plays a crucial role in the subsequent formation of ZnO/graphene. By studying the adsorption behavior, we gain insights into the binding energies, charge transfer processes, and possible changes in the electronic structure, all of which are essential for understanding the stability and functionality of the ZnO/G. In order to estimate the stability of ZnO coated graphene layer at various sites, the molecular models of ZnO and graphene are shown in Fig. 5(a, b), the bond lengths being for Zn-O (1.992 Å) and for C-C (1.419 Å). The adsorption energies for three type specific sites of ZnO on graphene monolayer were taken into account Fig. 5(c-e)): ZnO on the top of the carbon atom (Top-site), on the mid of the C-C bond (Bridge-site), and on the center of the hexagon (Hollow-site), the values being listed in Table 1. The calculation formula of the adsorption energy of ZnO on the G layer is defined as follows [51,52]:

$$\mathbf{E_{ad}} = \mathbf{E_{T(ZnO/G)}} - \mathbf{E_G} - \mathbf{E_{ZnO}}$$

where $\boldsymbol{E_{T(ZnO/G)}}$ represents the total energy of the ZnO adsorbent on the graphene layer, $\boldsymbol{E_G}$refers to the energy of the graphene monolayer and $\boldsymbol{E_{ZnO}}$corresponds to the energy of a ZnO molecule.

The angle and the length of the Zn-O bond are 108.04° and 1.99 Å, respectively, which are very close to the previous theoretical results [26,35,53]. As is well-known, the structure is more stable when the adsorption energy is lower, otherwise being unstable. According to Table 1, ZnO/ G (T-site) has the minimum adsorption energy, − 1.93983 eV, versus ZnO/G (B-site), and ZnO/G (H-site). In addition, the Zn atom is located at 1.797 Å from the nearest carbon atom, which closely matches the Van der Waals equilibrium spacing of 3.133 Å, as reported by Hu et al. [54]. As a result, when ZnO is coated onto the graphene monolayer, the C-C bond length increases slightly, while the Zn-O bond length changed slightly, which weakens the C-C bond strength bond.

4.2. Charge density difference

In order to investigate the interaction between graphene surface and the adsorbed ZnO molecule; we calculate the charge density difference for the three position as shown in Fig. 6, where the charge loss and the charge gain around atoms are represented by yellow and sky-blue color lobes, respectively.(see Fig. 6(b)).

The differential charge density was calculated by the following equation:

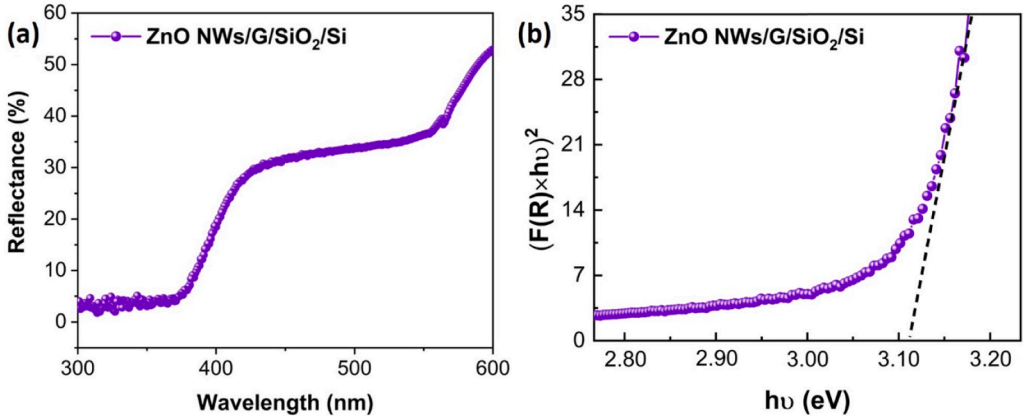

Fig. 4. (a) Reflectance spectra of ZnO NWs/G/SiO_2/Si; (b) Kubelka–Munk function versus photon energy of ZnO NWs/G/SiO_2/Si nanohybrid.

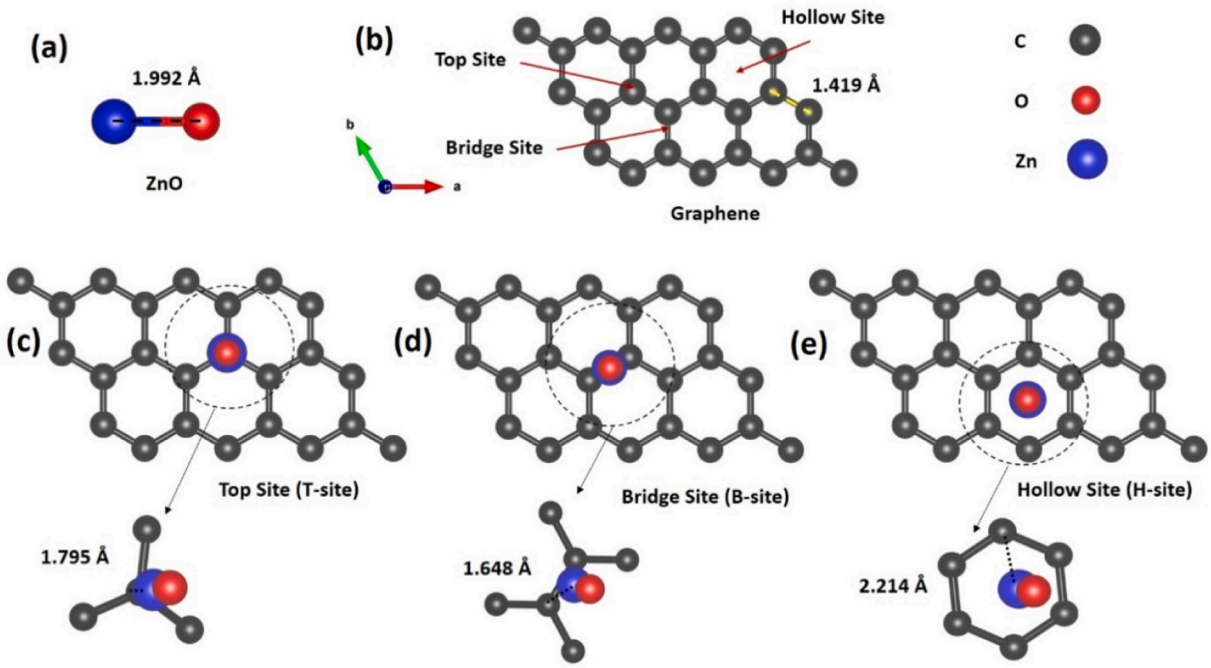

Fig. 5. Molecular models of ZnO (a) and graphene (b). Top views of the model adsorption structure; (c) ZnO/G (Bridge site), (d) ZnO/G (Top site), and (e) ZnO/G (Hollow site).

Table 1
Total energy, adsorption energy, Zn-C distance and schematic representation of ZnO/G composites: B-site, T-site and H-site, respectively.

Structures	$E_{T(ZnO/G)}$ (eV)	E_{ad} (eV)	Distance (Å)
ZnO/G (T-site)	-4935.81569	-1.93983	1.795
ZnO/G (B-site)	-4935.81183	-1.93597	1.648
ZnO/G (H-site)	-4935.78697	-1.91111	2.214

$$\Delta\rho = \rho(\mathbf{graphene} + \mathbf{ZnO}) - \rho(\mathbf{graphene}) - \rho(\mathbf{ZnO})$$

As we can see in Fig. 6, a significant amount of electron transfer took place between the ZnO molecule and the graphene monolayer in all three adsorption positions, indicating that the interaction between them is much stronger. Indeed, the oxygen atoms has lost charge in favor of the Zn and carbon atoms on the surface. In fact, the accumulation of charge between the ZnO molecule and the carbon atoms is greater on the two, hollow, and top, sites than on the bridge site. According to the Bader charge analysis, the bridge, top, and hollow sites exhibit transferred charges of −0.245 |e|, −0.545 |e|, and −0.338 |e|, respectively, indicating that the adsorbed ZnO molecule has lost a large amount of net charge on the top site. Hence, based on the adsorption energies given above, it can be concluded that the preferred site for ZnO molecule adsorption is the top site.

4.3. Electronic structure properties

After finding the most stable geometry of ZnO NWs/G, we firstly optimized a 2 × 2 × 2 supercell of ZnO ($Zn_{16}O_{16}$) crystallized in a hexagonal wurtzite structure (Fig. 7(a)), which belongs to the space group P63mc and has lattice parameters a = b = 3.249 Å and c = 5.215 Å (α = β = 90° and γ = 120°). Clearly, the computational results are in good agreement with the experimental results [15,55,56] as well as with the present findings. In fact, the deviation in lattice parameters between

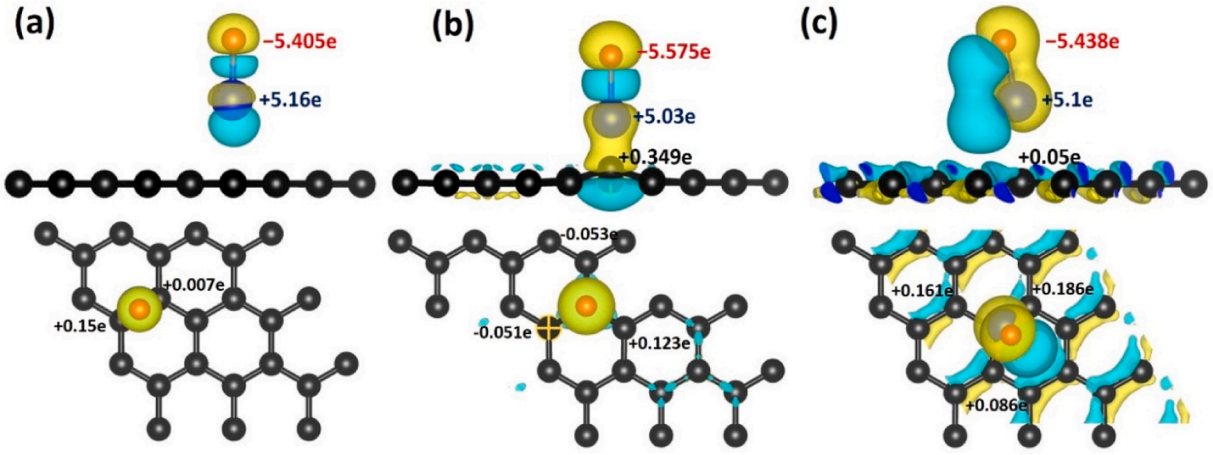

Fig. 6. (a) ZnO/G (Bridge site), (b) ZnO/G (Top site), and (c) ZnO/G (Hollow site) model adsorption structures; The isosurface value for the spin charge is 0.005 e/Å^3.

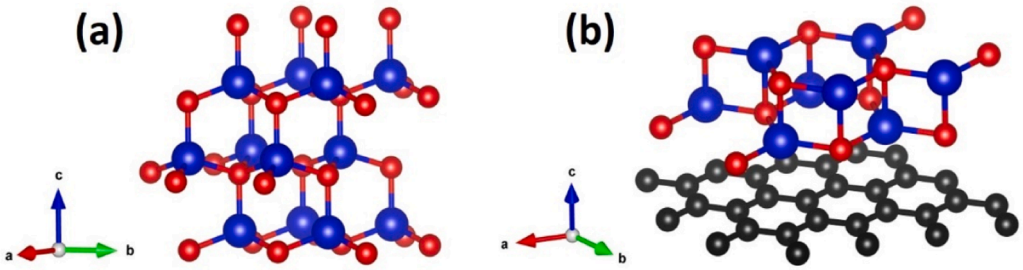

Fig. 7. Schematic representation of the structure of (a) ZnO NWs (b) ZnO NWs/graphene layer; the Zn atoms are marked with blue spheres, the O atoms with red spheres and the C atoms with black spheres.

the calculated and standard values (ICDD PDF no.00–036–1451) was less than 1%, suggesting that our calculations after optimization are reliable and demonstrate the validity of our model. Recently, a lot of research has been carried out on composite materials consisting mainly of graphene and metal oxides [57,58].

The combination of these components with new physical properties leads to a wide range of optoelectronic applications. In this study, we optimized a supercell of ZnO which is already built on graphene layer (Fig. 7(b)). According to our DFT calculations, ZnO prefers to be perpendicular to the graphene plane, with the Zn atom on the top of C–C bonds. Furthermore, the optimized cell parameters and distances between atoms in ZnO and ZnO/G composites are listed in Table 2.

The electronic properties of ZnO NWs and ZnO NWs coated graphene layer in the Top-site case are plotted to estimate the effect of graphene layer on the band structure of ZnO (Fig. 8). Furthermore, a schematic description of the gap energy of ZnO and ZnO NWs on graphene is given in Fig. 9. For pure ZnO, the band structures and density of states (TDOS and PDOS) of ZnO NWs are shown in Fig. 8(a, b), respectively. As can be seen in Fig. 8(a), the valence band maximum (MVB) occurs at Fermi level at 0eV, as directed by the Oxygen O-2p orbits, whereas the minimum of the conduction band (MCB) lies at G point and is dominated by Zn-4 s orbits (see Fig. 9(a)). Both MVB and MCB are located at G points of the Brillouin zone, confirming that ZnO has a direct band gap. From DFT calculations, for pure ZnO, only an approximate band gap of 0.74 eV may be obtained. This is far from that of 3.37 eV experimentally obtained [51,52]. We therefore found 3.37 eV of pure ZnO using the GGA+U method, with $U_O(2p) = 9$ eV and $U_{Zn}(3d) = 10$ eV, avoiding the commonly lower value in the band gap calculation caused by the DFT method. These results are in accordance with the experimental and theoretical results [59–62].

Furthermore, Fig. 8(b) shows the total density of states (TDOS) and partial density of states (PDOS) of pure ZnO, which combines both spin-up and spin-down channels, showing that the valence band is essentially composed of contributions from O-2p, O-2s and Zn-3d orbits. The conduction band mainly consists of O-2p, Zn-4s and Zn-4p orbits. Between 16 and 0 eV, the valence band is separated into three sections. In the lower energy part of the VB from − 15.5 to − 13.8 eV is mostly composed of the O-2s orbits with a small contribution of Zn-3d orbits. Within the region of 8.8 to − 5.4 eV shows sharp and tight peaks which are mainly formed of Zn-3d and partial O-2p orbits. The upper region of − 5.4–0 eV consists mainly of the O-2p orbits with a partial contribution of Zn-3d, as a result of d-p coupling. Further, the components of the conduction band contain the Zn-4s, Zn-4p orbits and small contribution of O-2p orbits.

Fig. 8(c, d) presents the electronic properties of ZnO NWs-coated graphene in the top-site case. The total density of states (TDOS) and partial density of states (PDOS), combining both spin-up and spin-down channels, shown in Fig. 8(d) indicate that the VB is dominated by 3d orbits of Zn and 2p and 2s orbits of O and C, whereas the CB is dominated by 2p and 2s orbits of C, 2p orbits of O and 4s and 3d orbits of Zn. It can be observed from Fig. 8(c), after the introduction of the graphene monolayer, that the electronic properties in the range of − 20–20 eV are modified, causing the appearance of new transition defects around the Fermi level. In fact, this type of defect corresponds to the transition of electrons from graphene to pure ZnO due to the presence of carbon defects [63].

The introduction of graphene causes the displacement of VBs and CBs to lower energy regions, affecting the electronic contribution positions of the orbitals with respect to pure ZnO, and resulting in a gap energy of 3.10 eV, this energy arising from the VBM (O-2p) and CBM (Zn-4 s) separation. This value of the gap energy ($E_{g:ZnO\ NWs/G}$), could equally be caused by the hybridization of O 2p and C 2p orbits shown in Fig. 8(d). Furthermore, based on Fig. 9(b) coupled with the PDOS analysis (Fig. 8(d)), part of 2p orbits of the carbon atom contribute to the occupied orbits near the Fermi level, causing the reduction of the band gap energy between the VB and CB, which is due to a large concentration of electrons placed in the conduction band (CB) which can reduce the band gap when ZnO is coated in the top-site on graphene layer. Our results demonstrate that the calculated band gap value of ZnO NWs coating a graphene layer using GGA+U is about 3.10 eV, which is lower than pure ZnO and is consistent with the experimental value obtained from the slopes of the diffuse reflectance (R) spectra (Fig. 4(b)). The decrease on the electronic band gap could be also attributed to the stacking of graphene layer with ZnO NWs, resulting in the energy level division near the Fermi level [64]. In addition, the Dirac cone of graphene (zero band gap) is clearly seen from Fig. 9(c). Our study of the electronic characteristics of ZnO NWs and ZnO NWs/G reveals that the decrease in the band gap is due mainly to the appearance of new transition defects around the Fermi level. Secondly, due to the presence of these carbon defects, the positions of the electronic contributions of the orbitals are modified compared to pure ZnO NWs, resulting in an upward shift of the bottom of CB and a downward shift of the top of VB.

Table 2
Calculated cell parameters, volume, total energy and equilibrium distances of ZnO NWs and ZnO NWs/ G nanohybrid.

	Cell parameters			
	a (Å)	c (Å)	Volume (Å^3)	Total energy (eV)
ZnO NWs	3.249	5.215	47.696	-4292.57
ZnO NWs/G	3.354	5.316	51.732	-4447.12

4.4. Optical properties

The optical properties of ZnO NWs and ZnO NWs/G, such as the complex dielectric function ($\varepsilon(\omega)$), reflectivity ($R(\omega)$), absorption coefficient ($\alpha(\omega)$) and optical conductivity are quantitatively calculated. In this context, the dielectric function is regarded as the fundamental and most significant characteristic for assessing other optical properties. The complex dielectric function is defined using the relation:

$$\varepsilon(\omega) = \varepsilon_1(\omega) + i\varepsilon_2(\omega)$$

The values of the real part $\varepsilon_1(\omega)$ are calculated from the imaginary part $\varepsilon_2(\omega)$ of the dielectric function using the Kramers-Kronig relations

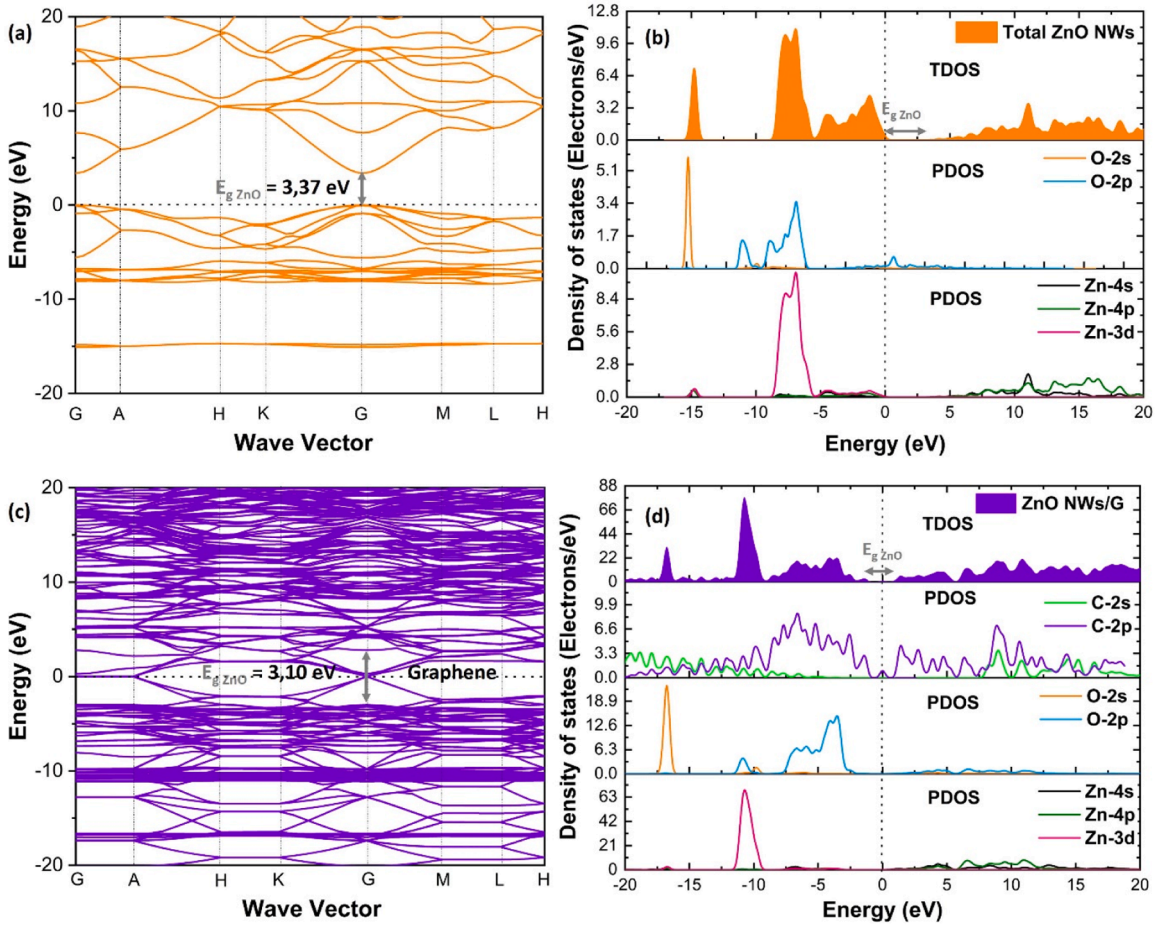

Fig. 8. (a) and (c) Band structures of ZnO NWs and ZnO NWs/G, respectively; (b) and (d) Total and partial density of states (DOS) of ZnO NWs and ZnO NWs/G, respectively; The Fermi level is set to 0 for both the band structures and the total and partial densities of states of ZnO NWs and ZnO NWs/G nanohybrid.

[65].

$$\varepsilon_1(\omega) = 1 + \frac{2}{\pi} P \int_0^{\infty} \frac{\varepsilon_2(\omega')\omega'}{\omega'^2 - \omega^2} d\omega$$

$$\varepsilon_2(\boldsymbol{\omega}) = \frac{2\pi e^2}{\Omega \varepsilon_0} \sum_{k,v,c} \langle \Psi_k^c | u \ \ r | \Psi_k^v \rangle^2 \delta(E_k^c - E_k^v - E)$$

where ω, P, u, Ω, e and k are the incident photon frequency, the main value of the integral, the polarization of incident electric filed, the unit cell volume, the electronic charge and the reciprocal lattice vector, respectively. The valence band is denoted by the superscript *v*, while the conduction band is represented by the superscript c. Therefore, the absorption coefficient $\boldsymbol{\alpha}(\boldsymbol{\omega})$, and reflectivity $\mathbf{R}(\boldsymbol{\omega})$ are described respectively using the relations:

$$\alpha(\omega) = \frac{\sqrt{2}\omega}{C_0} \left[\sqrt{\varepsilon_1(\omega)^2 + \varepsilon_2(\omega)^2} - \varepsilon_1(\omega) \right]^{1/2}$$

$$R(\omega) = \left| \frac{\sqrt{\varepsilon_1(\omega) + i\varepsilon_2(\omega)} - 1}{\sqrt{\varepsilon_1(\omega) + i\varepsilon_2(\omega)} + 1} \right|^2$$

where c_0 is the speed of light in vacuum.

For a more detailed analysis of the optical properties of ZnO NWs and ZnO NWs/G system, it was necessary to calculate the complex optical conductivity σ(ω) being given by [66]:

$$\sigma(\omega) = \sigma_1(\omega) + i\sigma_2(\omega)$$

$$\sigma_1(\omega) = 2nk\left(\frac{\omega}{4\pi}\right)$$

$$\sigma_2(\omega) = \left[1 - \left(n^2 - k^2\right)\right]\left(\frac{\omega}{4\pi}\right)$$

4.4.1. Dielectric function

To confirm the optical absorption properties and to explain the electronic transitions under the operating conditions, the imaginary part $\varepsilon_2(\omega)$ of the complex dielectric function is presented in Fig. 10. For ZnO, it can be observed that the dispersion spectrum starts to increase at around 2.2 eV in the visible region and approaches its maximum value of 2.94 at ~15.53 eV in the UV region. Three major peaks appear around 3.2–4.5 eV, 6.5–10 eV and 15.53 eV. The first peak at 3.2–4 eV is due to the electronic transitions in the highest VB (O-2p) to the lowest BC (Zn-4s) [67]. The second and third peaks mainly arise from direct electronic transitions between Zn-3d in the VB to O-2p and Zn-3d of VB to O-2s of CB respectively [62]. For ZnO NWs coated graphene layer, a new peak at 2.98 eV with a maximum value of 5.60 appeared. This appearance is associated to the direct electronic transitions from the O-2p to C-2p states [68]. As compared with ZnO NWs, the optical transition shift suggests that the band gap energy is reduce, which is consistent with the band structure results. Moreover, the $\varepsilon_2(\omega)$ curve increases in the UV and visible range after coating ZnO NWs on the graphene layer, owing to the electronic transitions of C-2p states in the CB.

4.4.2. Absorption, reflectivity and optical conductivity

The calculated absorption and reflectivity spectra versus incident

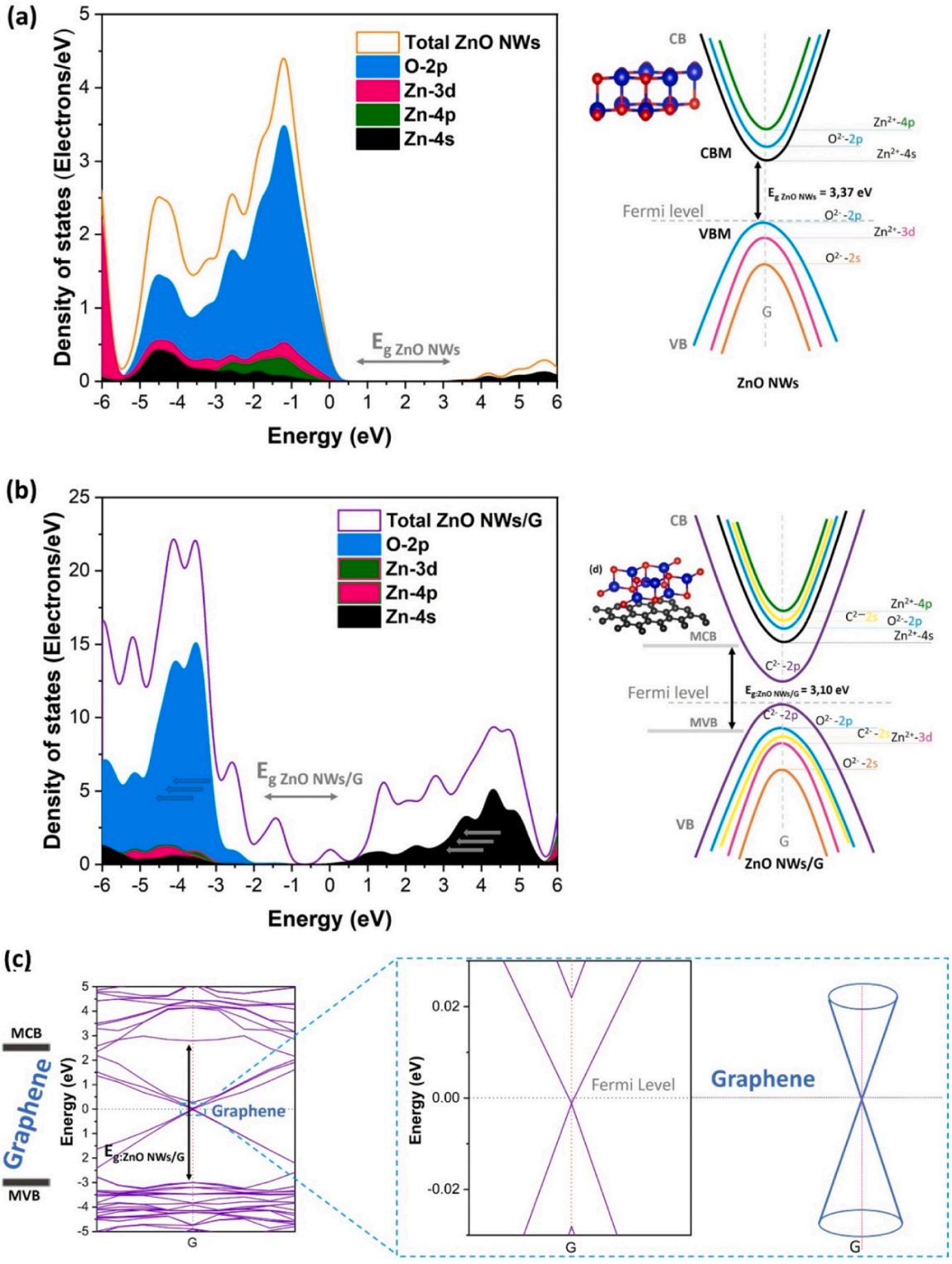

Fig. 9. (a, b) Schematic description of the gap energy of ZnO NWs and ZnO NWs/G nanohybrid, respectively and (c) schematic description of Dirac cone formation; The Fermi level is set to 0 eV for both the band structures and the total and partial densities of states of ZnO NWs and ZnO NWs/G nanohybrid.

photon energy of ZnO and ZnO NWs/G are ploted in Fig. 11. As given in Fig. 11(a), ZnO exhibits a maximum absorption peak of approximately 15.5 eV. Most of the absorption intensities of ZnO are confined to the ultraviolet region, owing to the low Zn-4s orbits in its conduction band minimum (see Fig. 8(b)) and its wide band gap. In addition, the absence of photo absorption in visible region for ZnO NWs is caused by the large value of the band gap (3.37 eV). The optical absorption of the ZnO NWs/G is enhanced compared to the ZnO NWs with the appearance absorption peak in the visible range around 1.5 eV. These absorption properties of ZnO NWs/G of reveal an excellent visible light response. In addition, the absorption curve shifted to lower energy regions from 16.6 eV for ZnO to 15.8 eV for ZnO NWs/G. This red shift obtained in our work is

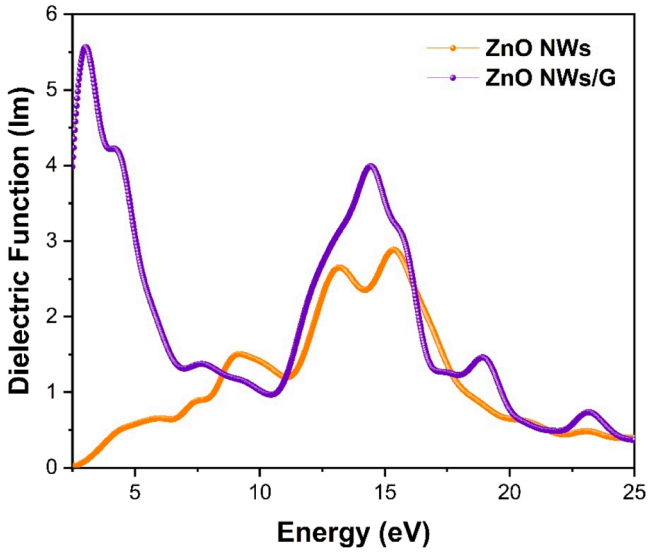

Fig. 10. The imaginary part of the dielectric function of ZnO NWs and ZnO NWs/ G nanohybrid.

due to the electron transition from the O-2p to the C-2p orbits (Fig. 8(d)). Furthermore, the observed red shift in the absorption spectra of ZnO NWs/G induced by electron transitions from O-2p to C-2p orbits represents a promising way to tune the optical properties of the material. This tunability improves the adaptability of ZnO NWs/G in various applications. For example, it proves to be extremely advantageous in photocatalytic processes, as the increased absorption leads to the generation of more electron-hole pairs, which leads to higher photocatalytic activity. Fig. 11(b) revealing that the reflectivity of ZnO NWs is less than 0.07 in the visible region and increases in the UV region with a maximum peak value of 0.25 at around 17.21 eV. For the ZnO NWs coated graphene layer, the reflectivity of ZnO NWs/G is higher than that of ZnO in the range 0–25 eV and shifts in the visible light direction with the maximum reflectivity peak value of 0.98 at 1.97 eV.

In Fig. 11(c, d), the real $\sigma_1(\omega)$ and imaginary $\sigma_2(\omega)$ parts of the optical conductivity for ZnO NWs and ZnO NWs/ G are presented as a function of photon energy. For both cases, the optical conductivity in the visible and UV ranges of ZnO on graphene layer is higher than that of ZnO, the first peak of $\sigma_1(\omega)$appearing at 3.10 eV which corresponds to the bandgap of ZnO NWs/G nanohybrid. The higher energy peaks of the ZnO NWs/G shifted toward a lower energy region observed for the ZnO NWs. As a result, the photoconductivity of ZnO NWs/G increases in the visible region due to the enhanced optical absorption. This confirms that graphene as a supporting substrate has enhanced the specific optoelectronic properties of ZnO NWs. This is most likely caused by the existence of defects, leading to an increase in total electron transfer and an increase in optical conductivity. Therefore, the higher optical conductivity in the visible region means that ZnO NWs/G are suitable for various optoelectronic applications, such as: light-emitting diodes (LEDs), solar cells and photovoltaic devices, in which efficient charge transport and efficient absorption in the visible spectrum occur, are crucial.

5. Conclusion

ZnO nanowires on graphene heterostructures were prepared by combining the CVD method with electrochemical deposition and transfer procedure. The obtained experimental results revealed that the ZnO nanowires crystallize in a wurtzite structure with a favored orientation along the c-axis (002), being dense, homogeneous, and almost

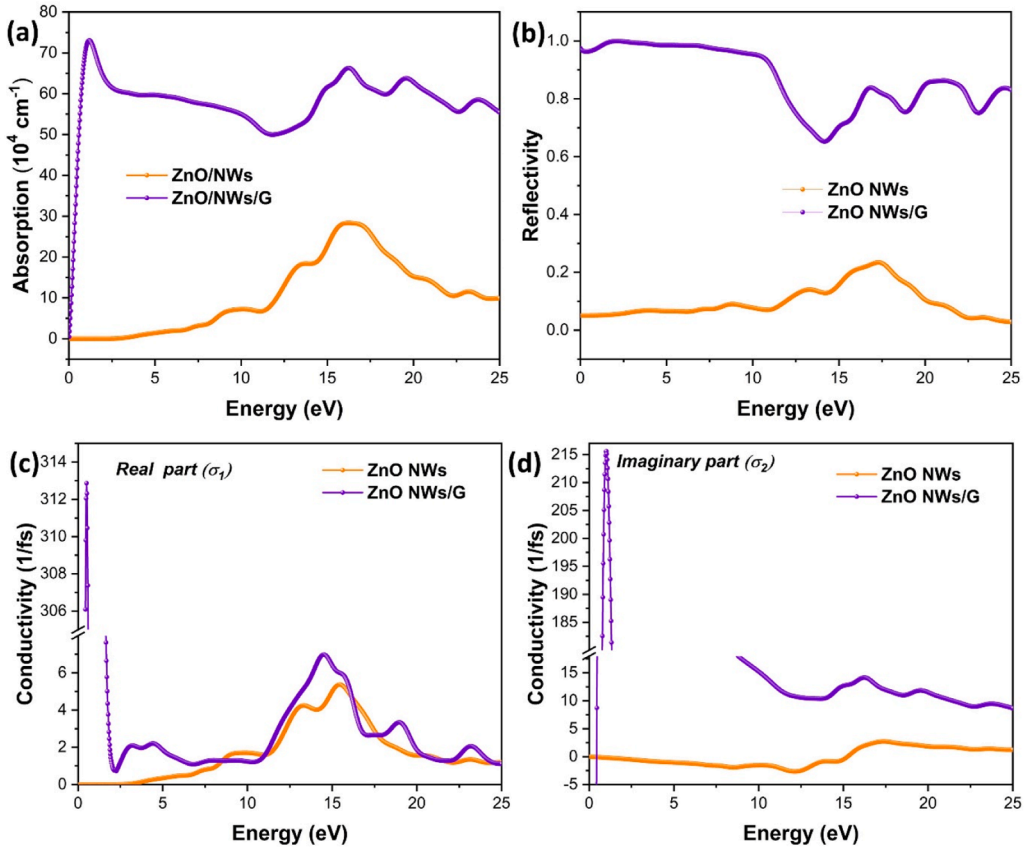

Fig. 11. The optical properties (a) absorption and (b) reflectivity, the calculated real part (a) and imaginary part (b) of the complex optical conductivity of ZnO NWs and ZnO NWs/G nanohybrid.

vertically aligned on the graphene layer. Most of the prepared nanowires have diameters between 20 and 40 nm and lengths from 100 to 300 nm. It was found that the coupling of the ZnO nanowires with the graphene layer reduced the band gap of ZnO. Further, using the DFT study, under GGA-PBE+ U and DFT-D2 methods, the density of states, band structures and optical properties of ZnO NWs/G were calculated. The adsorption energy shows that the structure of the ZnO top site on graphene layer is more stable. Further, it was found that ZnO NWs/G nanohybrids have an enhancement in optical properties and optical conductivity in the UV and visible light ranges compared to ZnO. We assume that the present study will provide consistent fundament for understanding the potential of ZnO NWs/G nanohybrids in optoelectronic devices, especially in sensor applications and will inspire additional research.

CRediT authorship contribution statement

Enculescu Ionut: Conceptualization, Formal analysis, Methodology, Writing – original draft, Writing – review & editing. **Matei Elena:** Conceptualization, Data curation, Formal analysis, Funding acquisition, Investigation, Methodology, Project administration, Resources, Supervision, Writing – original draft, Writing – review & editing. **Boukhoubza Issam:** Conceptualization, Data curation, Formal analysis, Investigation, Writing – original draft, Writing – review & editing. **Achehboune Mohamed:** Writing – Theoretical calculations original draft preparation. **Derkaoui Issam:** Conceptualization, Formal analysis, Writing – original draft preparation. **Apostol Mariana Mihaela:** Formal analysis, Investigation, Writing – original draft, Writing – review & editing. **Basyooni Mohamed A.:** Formal analysis, Investigation, Writing – original draft, Writing – review & editing. **Khenfouch Mohammed:** Formal analysis, Investigation, Writing – original draft, Writing – review & editing. **Nedelcu Liviu:** Formal analysis, Investigation, Writing – original draft, Writing – review & editing.

Declaration of Competing Interest

The authors declare that they have no known competing financial interests or personal relationships that could have appeared to influence the work reported in this paper.

Data availability

Data will be made available on request.

Acknowledgements

I.B. acknowledges the Romanian Ministry of Foreign Affairs and the Agence Universitaire de la Francophonie for the Eugen Ionescu research and mobility grant at the National Institute of Materials Physics. M.M.A. acknowledges the grant POCU/993/6/13−153178, co-financed by the European Social Fund within the Sectorial Operational Program Human Capital 2014 – 2020. This research was supported by Core Program of the National Institute of Materials Physics, granted by the Romanian Ministry of Research, Innovation and Digitalization under the Project PC1-PN23080101 and PCCE 45/2021.

References

[1] R.R. Nair, P. Blake, A.N. Grigorenko, K.S. Novoselov, T.J. Booth, T. Stauber, N. M. Peres, A.K. Geim, Fine structure constant defines visual transparency of graphene, Science 320 (2008) 1308-1308.
[2] A.A. Balandin, S. Ghosh, D. Teweldebrhan, I. Calizo, W. Bao, F. Miao, C.N. Lau, 2008. Extremely high thermal conductivity of graphene: prospects for thermal management applications in silicon nanoelectronics, in: 2008 IEEE Silicon Nanoelectronics Workshop, IEEE. 1–2.
[3] A.K. Geim, K.S. Novoselov, The rise of graphene, Nat. Mater. 6 (2007) 183–191.
[4] V. Mazánek, J. Luxa, S. Matějková, J. Kučera, D. Sedmidubský, M. Pumera, Z. Sofer, Ultrapure graphene is a poor electrocatalyst: definitive proof of the key role of metallic impurities in graphene-based electrocatalysis, ACS Nano 13 (2019) 1574–1582.
[5] L. Xie, X. Zi, Q. Meng, Z. Liu, L. Xu, Detection of physiological signals based on graphene using a simple and low-cost method, Sensors 19 (2019) 1656.
[6] S.S. Gunasekaran, T.K. Kumaresan, S.A. Masilamani, S.Z. Karazhanov, K. Raman, R. Subashchandrabose, Divulging the electrochemical hydrogen storage on nitrogen doped graphene and its superior capacitive performance, Mater. Lett. 273 (2020), 127919.
[7] R. Wang, Y. Mao, L. Wang, H. Qu, Y. Chen, L. Zheng, Solution-gated graphene transistor based sensor for histamine detection with gold nanoparticles decorated graphene and multi-walled carbon nanotube functionalized gate electrodes, Food Chem. 347 (2021), 128980.
[8] S. Zhang, Z. Li, F. Xing, Review of polarization optical devices based on graphene materials, Int. J. Mol. Sci. 21 (2020) 1608.
[9] I. Derkaoui, M. Khenfouch, B.M. Mothudi, A. Jorio, Zorkani, I.M. Maaza, PH effect on the optoelectronic properties of graphene vanadium oxides nanocomposites, J. Mater. Sci. Mater. Electron 28 (2017) 17710–17718.
[10] X. Li, W. Cai, J. An, S. Kim, J. Nah, D. Yang, R. Piner, A. Velamakanni, I. Jung, E. Tutuc, Large-area synthesis of high-quality and uniform graphene films on copper foils, Science 324 (2009) 1312–1314.
[11] J. Čermák, T. Yamada, M. Ledinskỳ, M. Hasegawa, B. Rezek, Microscopically inhomogeneous electronic and material properties arising during thermal and plasma CVD of graphene, J. Mater. Chem. C. 2 (2014) 8939–8948.
[12] A. Janotti, C.G. Van de Walle, Fundamentals of zinc oxide as a semiconductor, Rep. Prog. Phys. 72 (2009), 126501.
[13] D.C. Look, Recent advances in ZnO materials and devices, Mater. Sci. Eng. B. 80 (2001) 383–387.
[14] J. Cui, Zinc oxide nanowires, Mater. Charact. 64 (2012) 43–52.
[15] M. Achehboune, M. Khenfouch, I. Boukhoubza, B.M. Mothudi, I. Zorkani, A. Jorio, Holmium (Ho)-coated ZnO nanorods: an investigation of optoelectronic properties, J. Mater. Sci. Mater. Electron 31 (2020) 4595–4604.
[16] P. Samadipakchin, H.R. Mortaheb, A. Zolfaghari, ZnO nanotubes: preparation and photocatalytic performance evaluation, J. Photochem. Photobiol. Chem. 337 (2017) 91–99.
[17] Y. Qu, R. Huang, W. Qi, M. Shi, R. Su, Z. He, Controllable synthesis of ZnO nanoflowers with structure-dependent photocatalytic activity, Catal. Today 355 (2020) 397–407.
[18] T. Iqbal, M.A. Khan, H. Mahmood, Facile synthesis of ZnO nanosheets: structural, antibacterial and photocatalytic studies, Mater. Lett. 224 (2018) 59–63.
[19] J. Xu, Y. Cui, Y. Han, M. Hao, X. Zhang, ZnO–graphene composites with high photocatalytic activities under visible light, RSC Adv. 6 (2016) 96778–96784.
[20] E.R. Ezeigwe, M.T. Tan, P.S. Khiew, C.W. Siong, One-step green synthesis of graphene/ZnO nanocomposites for electrochemical capacitors, Ceram. Int. 41 (2015) 715–724.
[21] J. Wu, M. Gong, ZnO/graphene heterostructure nanohybrids for optoelectronics and sensors, J. Appl. Phys. 130 (2021), 070905.
[22] M.M. Tavakoli, R. Tavakoli, P. Yadav, J. Kong, A graphene/ZnO electron transfer layer together with perovskite passivation enables highly efficient and stable perovskite solar cells, J. Mater. Chem. A 7 (2019) 679–686.
[23] I. Boukhoubza, E. Matei, A. Jorio, M. Enculescu, I. Enculescu, Electrochemical deposition of ZnO nanowires on CVD-graphene/copper substrates, Nanomaterials 12 (2022) 2858.
[24] S. Zhang, Y. Zhang, S. Huang, H. Liu, P. Wang, H. Tian, First-principles study of field emission properties of graphene-ZnO nanocomposite, J. Phys. Chem. C. 114 (2010) 19284–19288.
[25] W. Geng, X. Zhao, H. Liu, X. Yao, Influence of interface structure on the properties of ZnO/graphene composites: a theoretical study by density functional theory calculations, J. Phys. Chem. C. 117 (2013) 10536–10544.
[26] M. Achehboune, M. Khenfouch, I. Boukhoubza, I. Derkaoui, L. Leontie, A. Carlescu, B.M. Mothudi, I. Zorkani, A. Jorio, Optimization of the luminescence and structural properties of Er-doped ZnO nanostructures: effect of dopant concentration and excitation wavelength, J. Lumin. 246 (2022), 118843.
[27] I. Derkaoui, M. Achehboune, I. Boukhoubza, R. Hatel, Z. El Adnani, A. Rezzouk, Investigation of the crystal structure, electronic and optical properties of Cr-doped BaTiO3 on the Ti site using first principles calculations, J. Phys. Chem. Solids 175 (2023), 111209.
[28] P. Makkar, N.N. Ghosh, A review on the use of DFT for the prediction of the properties of nanomaterials, RSC Adv. 11 (2021) 27897–27924.
[29] I. Derkaoui, M. Achehboune, I. Boukhoubza, Z. El Adnani, A. Rezzouk, Improved first-principles electronic band structure for cubic ($Pm\bar{3}m$) and tetragonal (P4mm, P4/mmm) phases of BaTiO3 using the Hubbard U correction, Comput. Mater. Sci. 217 (2023), 111913.
[30] A. Alnuaimi, I. Almansouri, I. Saadat, A. Nayfeh, Toward fast growth of large area high quality graphene using a cold-wall CVD reactor, RSC Adv. 7 (2017) 51951–51957.
[31] Z. Tang, C. Neumann, A. Winter, A. Turchanin, Electrochemical delamination assisted transfer of molecular nanosheets, Nanoscale 12 (2020) 8656–8663.
[32] S.J. Clark, M.D. Segall, C.J. Pickard, P.J. Hasnip, M.I. Probert, K. Refson, M. C. Payne, First principles methods using CASTEP, Z. Für Krist. - Cryst. Mater. 220 (2005) 567–570.
[33] J.P. Perdew, K. Burke, M. Ernzerhof, Generalized gradient approximation made simple, Phys. Rev. Lett. 77 (1996) 3865.
[34] D. Vanderbilt, Soft self-consistent pseudopotentials in a generalized eigenvalue formalism, Phys. Rev. B. 41 (1990) 7892–7895.
[35] M. Achehboune, M. Khenfouch, I. Boukhoubza, I. Derkaoui, B.M. Mothudi, I. Zorkani, A. Jorio, A. DFT, study on the electronic structure, magnetic and optical

properties of Er doped ZnO: effect of Er concentration and native defects, Comput. Condens. Matter 31 (2022), e00627.
[36] S.J. Chae, F. Güneş, K.K. Kim, E.S. Kim, G.H. Han, S.M. Kim, H.-J. Shin, S.-M. Yoon, J.-Y. Choi, M.H. Park, Synthesis of large-area graphene layers on poly-nickel substrate by chemical vapor deposition: wrinkle formation, Adv. Mater. 21 (2009) 2328–2333.
[37] N.A. Hambali, A.M. Hashim, Synthesis of zinc oxide nanostructures on graphene/glass substrate via electrochemical deposition: effects of potassium chloride and hexamethylenetetramine as supporting reagents, Nano Micro Lett. 7 (2015) 317–324.
[38] P. Bindu, S. Thomas, Estimation of lattice strain in ZnO nanoparticles: X-ray peak profile analysis, J. Theor. Appl. Phys. 8 (2014) 123–134.
[39] H.D. Cho, D.Y. Kim, J.K. Lee, ZnO nanorod/graphene hybrid-structures formed on Cu sheet by self-catalyzed vapor-phase transport synthesis, Nanomaterials 11 (2021) 450.
[40] P.M.V. Raja, G.L. Esquenazi, D.R. Jones, J. Li, B.E. Brinson, K. Wright, C.E. Gowenlock, A.R. Barron, Electroless Deposition of Cu-SWCNT Composites, C. 5 (2019) 61.
[41] A.R. Nanakkal, L.K. Alexander, Photocatalytic activity of graphene/ZnO nanocomposite fabricated by two-step electrochemical route, J. Chem. Sci. 129 (2017) 95–102.
[42] M. Saranya, R. Ramachandran, F. Wang, Graphene-zinc oxide (G-ZnO) nanocomposite for electrochemical supercapacitor applications, J. Sci. Adv. Mater. Devices 4 (2016) 454–460.
[43] D.-H. Yoo, T.V. Cuong, V.H. Luan, N.T. Khoa, E.J. Kim, S.H. Hur, S.H. Hahn, Photocatalytic performance of a Ag/ZnO/CCG multidimensional heterostructure prepared by a solution-based method, J. Phys. Chem. C. 116 (2012) 7180–7184.
[44] H. Zeng, Y. Cao, S. Xie, J. Yang, Z. Tang, X. Wang, L. Sun, Synthesis, optical and electrochemical properties of ZnO nanowires/graphene oxide heterostructures, Nanoscale Res. Lett. 8 (2013) 133.
[45] C. Casiraghi, A. Hartschuh, H. Qian, S. Piscanec, C. Georgi, A. Fasoli, K. S. Novoselov, D.M. Basko, A.C. Ferrari, Raman spectroscopy of graphene edges, Nano Lett. 9 (2009) 1433–1441.
[46] E.K. Athanassiou, R.N. Grass, W.J. Stark, Large-scale production of carbon-coated copper nanoparticles for sensor applications, Nanotechnology 17 (2006) 1668.
[47] Z. Zhaochun, H. Baibiao, Y. Yongqin, C. Deliang, Electrical properties and Raman spectra of undoped and Al-doped ZnO thin films by metalorganic vapor phase epitaxy, Mater. Sci. Eng. B. 86 (2001) 109–112.
[48] R. Cuscó, E. Alarcón-Lladó, J. Ibanez, L. Artús, J. Jiménez, B. Wang, M.J. Callahan, Temperature dependence of Raman scattering in ZnO, Phys. Rev. B. 75 (2007), 165202.
[49] J. Hrubỳ, Š. Vavrečková, L. Masaryk, A. Sojka, J. Navarro-Giraldo, M. Bartoš, R. Herchel, J. Moncol, I. Nemec, P. Neugebauer, Deposition of tetracoordinate Co (II) complex with chalcone ligands on graphene, Molecules 25 (2020) 5021.
[50] F. Jahan, M.H. Islam, B.E. Smith, Band gap and refractive index determination of Mo-black coatings using several techniques, Sol. Energy Mater. Sol. Cells 37 (1995) 283–293.
[51] R. Gholizadeh, Y.-X. Yu, Y. Wang, N2O adsorption and decomposition over ZnO (0001) doped graphene: density functional theory calculations, Appl. Surf. Sci. 420 (2017) 944–953.
[52] H. Chen, Y. Qu, J. Ding, H. Fu, Adsorption behavior of graphene-like ZnO monolayer with oxygen vacancy defects for NO2: A DFT study, Superlattices Microstruct. 134 (2019), 106223.
[53] F.W. Fernandes, V.F.G. de Paiva, G.P. Thim, Energetic and electronic properties in a multilayered ZnO graphene-like nanostructure, Mater. Res. 19 (2016) 497–504.
[54] W. Hu, Z. Li, J. Yang, Electronic and optical properties of graphene and graphitic ZnO nanocomposite structures, J. Chem. Phys. 138 (2013), 124706.
[55] S. Al-Ariki, N.A. Yahya, S.A. Al-A′nsi, M.H. Jumali, A.N. Jannah, R. Abd-Shukor, Synthesis and comparative study on the structural and optical properties of ZnO doped with Ni and Ag nanopowders fabricated by sol gel technique, Sci. Rep. 11 (2021) 1–11.
[56] G. Madhumitha, J. Fowsiya, N. Gupta, A. Kumar, M. Singh, Green synthesis, characterization and antifungal and photocatalytic activity of Pithecellobium dulce peel–mediated ZnO nanoparticles, J. Phys. Chem. Solids 127 (2019) 43–51.
[57] I. Derkaoui, M. Khenfouch, B.M. Mothudi, A. Jorio, I. Zorkani, M. Maaza, PH effect on the optoelectronic properties of graphene vanadium oxides nanocomposites, J. Mater. Sci. Mater. Electron 28 (2017) 17710–17718.
[58] I. Boukhoubza, M. Khenfouch, M. Achehboune, L. Leontie, A.C. Galca, M. Enculescu, A. Carlescu, M. Guerboub, B.M. Mothudi, A. Jorio, Graphene oxide concentration effect on the optoelectronic properties of ZnO/GO nanocomposites, Nanomaterials 10 (2020) 1532.
[59] R.D. Vispute, V. Talyansky, S. Choopun, R.P. Sharma, T. Venkatesan, M. He, X. Tang, J.B. Halpern, M.G. Spencer, Y.X. Li, Heteroepitaxy of ZnO on GaN and its implications for fabrication of hybrid optoelectronic devices, Appl. Phys. Lett. 73 (1998) 348–350.
[60] L. Wang, N.C. Giles, Temperature dependence of the free-exciton transition energy in zinc oxide by photoluminescence excitation spectroscopy, J. Appl. Phys. 94 (2003) 973–978.
[61] J. Wang, T. Shen, Y. Feng, H. Liu, A. GGA, U study of electronic structure and the optical properties of different concentrations Tb doped ZnO, Phys. B Condens. Matter 576 (2020), 411720.
[62] Y.-S. Lee, Y.-C. Peng, J.-H. Lu, Y.-R. Zhu, H.-C. Wu, Electronic and optical properties of Ga-doped ZnO, Thin Solid Films 570 (2014) 464–470.
[63] A. Gong, T. Shen, Y. Feng, J. Chen, Z. Wang, Van der Waals heterostructure of graphene Defected&Doped X (X= Au, N) composite ZnO monolayer: a first principle study, Mater. Sci. Semicond. Process. 138 (2022), 106247.
[64] W. Wei, S. Yang, G. Wang, T. Zhang, W. Pan, Z. Cai, Y. Yang, L. Zheng, P. He, L. Wang, Bandgap engineering of two-dimensional C3N bilayers, Nat. Electron. 4 (2021) 486–494.
[65] L. Li, W. Wang, H. Liu, X. Liu, Q. Song, S. Ren, First principles calculations of electronic band structure and optical properties of Cr-doped ZnO, J. Phys. Chem. C. 113 (2009) 8460–8464.
[66] R. Khenata, A. Bouhemadou, M. Sahnoun, A.H. Reshak, H. Baltache, M. Rabah, Elastic, electronic and optical properties of ZnS, ZnSe and ZnTe under pressure, Comput. Mater. Sci. 38 (2006) 29–38.
[67] J.-H. Luo, Q. Liu, L.-N. Yang, Z.-Z. Sun, Z.-S. Li, First-principles study of electronic structure and optical properties of (Zr–Al)-codoped ZnO, Comput. Mater. Sci. 82 (2014) 70–75.
[68] F. Opoku, K.K. Govender, C.G.C.E. van Sittert, P.P. Govender, Understanding the mechanism of enhanced charge separation and visible light photocatalytic activity of modified wurtzite ZnO with nanoclusters of ZnS and graphene oxide: from a hybrid density functional study, N. J. Chem. 41 (2017) 8140–8155.